entropy

MDPI

Article

Exploring the Neighborhood of q-Exponentials

Henrique Santos Lima [1,*] and Constantino Tsallis [1,2,3,4]

[1] Centro Brasileiro de Pesquisas Físicas, Rua Xavier Sigaud 150, Rio de Janeiro, RJ 22290-180, Brazil; tsallis@cbpf.br
[2] National Institute of Science and Technology of Complex Systems, Rua Xavier Sigaud 150, Rio de Janeiro, RJ 22290-180, Brazil
[3] Santa Fe Institute, 1399 Hyde Park Road, Santa Fe, NM 87501, USA
[4] Complexity Science Hub Vienna, Josefstädter Strasse 39, 1080 Vienna, Austria
* Correspondence: hslima94@cbpf.br

Received: 18 November 2020; Accepted: 7 December 2020; Published: 11 December 2020

Abstract: The q-exponential form $e_q^x \equiv [1+(1-q)x]^{1/(1-q)}$ $(e_1^x = e^x)$ is obtained by optimizing the nonadditive entropy $S_q \equiv k\frac{1-\sum_i p_i^q}{q-1}$ (with $S_1 = S_{BG} \equiv -k\sum_i p_i \ln p_i$, where BG stands for Boltzmann–Gibbs) under simple constraints, and emerges in wide classes of natural, artificial and social complex systems. However, in experiments, observations and numerical calculations, it rarely appears in its pure mathematical form. It appears instead exhibiting crossovers to, or mixed with, other similar forms. We first discuss departures from q-exponentials within crossover statistics, or by linearly combining them, or by linearly combining the corresponding q-entropies. Then, we discuss departures originated by double-index nonadditive entropies containing S_q as particular case.

Keywords: q-exponentials; nonextensive statistical mechanics; nonadditive entropies; complex systems

1. Introduction

Nonadditive entropies have been used as a basis to explain a diversity of phenomena, from astrophysics to the oscillatory behavior of El Niño [1–3], from DNA to financial markets [4,5] from high-energy physics of collisions to granular matter and cold atoms [6–8], among many others. It turns out that wide classes of complex systems can be satisfactorily handled within a generalization of Boltzmann–Gibbs (BG) statistical mechanics based on the nonadditive entropy

$$S_q \equiv k\frac{1-\sum_{i=1}^W p_i^q}{q-1} = k\sum_{i=1}^W p_i \ln_q \frac{1}{p_i} \quad \left(q\in\mathbb{R};\, S_1 = S_{BG} \equiv -k\sum_{i=1}^W p_i \ln p_i;\, \sum_{i=1}^W p_i = 1\right), \tag{1}$$

where W is the total number of microstates and k is a conventional positive constant (usually $k = k_B$ in physics, and $k = 1$ in computational sciences), the q-logarithmic function being defined as $\ln_q z \equiv \frac{z^{1-q}-1}{1-q}$ $(\ln_1 z = \ln z)$. This theory is currently referred to as nonextensive statistical mechanics, or q-statistics for short [9–11]. The optimization of S_q with simple constraints yields

$$p_i = \frac{e_q^{-\beta_q E_i}}{\sum_{j=1}^W e_q^{-\beta_q E_j}}, \tag{2}$$

where $\{E_i\}$ are the energy eigenvalues, and the q-exponential function (inverse of the q-logarithmic function) is defined as follows:

$$e_q^x \equiv [1+(1-q)x]_+^{\frac{1}{1-q}} \quad (q\in\mathbb{R};\, e_1^x = e^x), \tag{3}$$

where $[z]_+ = z$ if $z > 0$ and zero if $z \leq 0$; notice that this definition implies that, for $q < 1$, there is a cutoff at $x_{cutoff} = -1/(1-q) < 0$ [9]. In the limit $q \to 1$, Equation (2) recovers the celebrated BG weight.

The aim of the present article is to discuss in detail some departures from a pure q-exponential function which frequently emerge in real situations. Such variations are used in the statistics of nucleotides in full genomes [4], the re-association of folded proteins [12], standard map for intermediate values of the control parameter [13], to mention but a few. We focus on crossover statistics (Section 2), linear combinations of q-exponential functions (Section 3), linear combinations of q-entropies (Section 4), and some two-indices entropies, namely $S_{q,\delta}$ [14], $S^{BR}_{q,q'}$ [15] and $S_{q,q'}$ [16] (Section 5).

2. Multiple Crossover Statistics

Crossover statistics is often useful whenever the phenomenon which is focused on exhibits a q-exponential behavior within a range of the relevant variables, and then makes a crossover to another q-exponential function with a different index q. Although rare, it can, in principle, happen that several crossovers successively occur one after the other. We will refer to it as *multiple crossover statistics*.

Illustrations of such crossovers can be found in [12,17–21].

Let us consider the following ordinary differential equation:

$$\frac{dy}{dx} = -a y^q \quad (y(0) = 1;\, a \in \mathbb{R})\,. \tag{4}$$

Its solution is given by

$$y(x) = e_q^{-a\,x}\,. \tag{5}$$

Multiple crossovers emerge from the following nonlinear ordinary differential equation:

$$\frac{dy}{dx} = -\sum_{k=1}^{M} a_k\, y^{q_k} \quad (q_1 < q_2 < \cdots < q_M)\,, \tag{6}$$

with $y(0) = 1$, and $0 \leq a_1 \leq a_2 \leq \cdots \leq a_M$, where the right-hand term is constituted by a linear combination of nonlinear terms. Consequently

$$x = \int_y^1 \frac{dz}{\sum_{k=1}^{M} a_k\, z^{q_k}}\,. \tag{7}$$

We know that Equation (7) has analytical solutions for $M = 1$ and $M = 2$ (Figure 1). For $M > 2$, we need to solve this equation numerically.

Particularly for crossover between two curves ($M = 2$) with q_1 and q_2, we have:

$$\frac{dy}{dx} = -a_1 y^{q_1} - a_2 y^{q_2} = -\mu_{q_1} y^{q_1} - (\lambda_{q_2} - \mu_{q_1}) y^{q_2} \quad (y(0) = 1)\,, \tag{8}$$

where we have identified $(a_1, a_2) \equiv (\mu_{q_1}, \lambda_{q_2} - \mu_{q_1})$ in order to facilitate the connection with the notation used in [12]. Let us incidentally mention that this equation enabled the study of the anomalous behavior of folded proteins.

To solve Equation (8), we use Equation (7), which yields

$$x = \frac{1}{\mu_{q_1}} \left\{ \frac{y^{1-q_1}-1}{q_1-1} - \frac{\left(\frac{\lambda_{q_2}}{\mu_{q_1}}\right)-1}{1+q_2-2q_1} \times \left[H\left(1; q_2-2q_1, q_2-q_1, \left(\frac{\lambda_{q_2}}{\mu_{q_1}}\right)-1\right) - H\left(y; q_2-2q_1, q_2-q_1, \left(\frac{\lambda_{q_2}}{\mu_{q_1}}\right)-1\right)\right]\right\} \tag{9}$$

with

$$H(y;a,b,c) = y^{1+a}\,{}_2F_1\left(\frac{1+a}{b}, 1; \frac{1+a+b}{c}; -y^b c\right), \tag{10}$$

where ${}_2F_1$ is a hypergeometric function.

For the particular case $q_1 = 1$, we obtain

$$y = \frac{1}{\left[1 - \frac{\lambda_{q_2}}{\mu_1} + \frac{\lambda_{q_2}}{\mu_1} e^{(q_2-1)\,\mu_1 x}\right]^{\frac{1}{q_2-1}}}. \tag{11}$$

It is certainly worth mentioning that its $q_2 = 2$ instance yields $y = \left[1 - \frac{\lambda_2}{\mu_1} + \frac{\lambda_2}{\mu_1} e^{\mu_1 x}\right]^{-1}$, whose $\lambda_2/\mu_1 >> 1$ asymptotic behavior becomes $y \propto 1/[e^{\mu_1 x} - 1]$. It is precisely through this ordinary-differential path that Planck found, in his historical 19 October 1900 paper, the thermostatistical factor which eventually led to his celebrated law for the black-body radiation with the ultimate identification $\mu_1 x \to h\nu/k_B T$ [22,23].

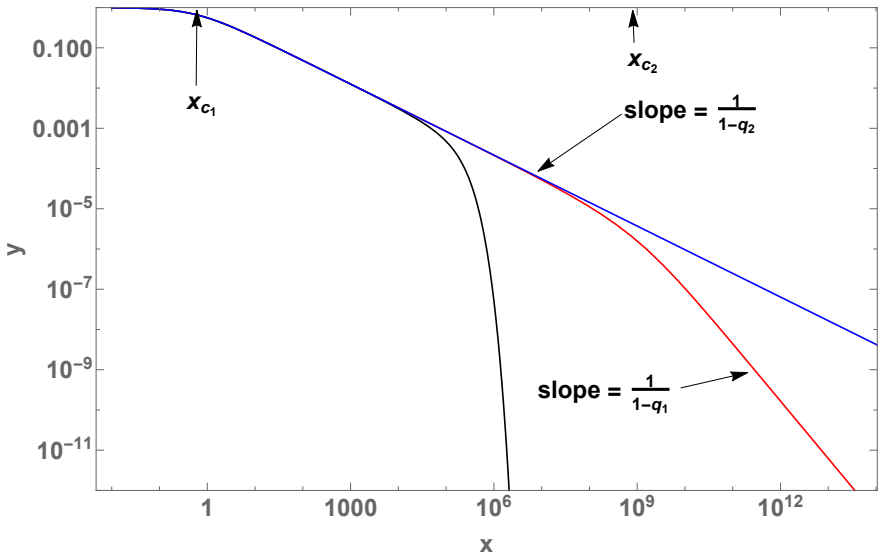

Figure 1. $y(x)$ (log-log plot). For the case $M = 1$ with $(q, a) = (2.7, 1)$ (blue curve) and, for the case $M = 2$, the crossover between two curves, namely with $q_1 = 1$ (black curve) and $q_1 = 1.7$ (red curve) respectively, both with $(q_2, \lambda_{q_2}, \mu_{q_1}) = (2.7, 1, 1 \times 10^{-5})$. For the red curve, we have the crossover characteristic values $(x_{c_1}, x_{c_2}) = (0.588, 8.407 \times 10^8)$, which indicate the passage from one regime to another.

For the case $M = 3$, we have

$$\frac{dy}{dx} = -a_1 y^{q_1} - a_3 y^{q_2} - a_3 y^{q_3} \tag{12}$$

whose analytical solution is intractable. Therefore, we use numerical methods to solve it. In contrast, the characteristic values $(x_{c_1}, x_{c_2}, x_{c_3})$ where changes of behavior of the curve occur are analytically accessible. Those values are obtained through the following considerations. For the characteristic value x_{c_1}, we have

$$y(x_{c_1}) \sim [(q_3 - 1)a_3 x_{c_1}]^{-\frac{1}{q_3 - 1}} \sim 1\,. \tag{13}$$

Consequently

$$x_{c_1} = \frac{1}{[(q_3 - 1)a_3]}\,. \tag{14}$$

For x_{c_2} we have

$$y(x_{c_2}) \sim [(q_2 - 1)a_2 x_{c_2}]^{-\frac{1}{q_2 - 1}} \sim [(q_3 - 1)a_3 x_{c_2}]^{-\frac{1}{q_3 - 1}}\,, \tag{15}$$

hence

$$x_{c_2} = \frac{[(q_3 - 1)a_3]^{\frac{q_2 - 1}{q_3 - q_2}}}{[(q_2 - 1)a_2]^{\frac{q_3 - 1}{q_3 - q_2}}}\,. \tag{16}$$

Similarly, we have

$$x_{c_3} = \frac{[(q_2 - 1)a_2]^{\frac{q_1 - 1}{q_2 - q_1}}}{[(q_1 - 1)a_1]^{\frac{q_2 - 1}{q_2 - q_1}}}\,. \tag{17}$$

Therefore, for the $M = 3$ particular case whose parameter values are $a_1 = 5 \times 10^{-11}$, $a_2 = 1 \times 10^{-4}$ and $a_3 = 1$, with $q_1 = 1.2$, $q_2 = 1.7$ and $q_3 = 2.7$, we have $x_{c_1} \approx 0.59$, $x_{c_2} \approx 1.68 \times 10^7$ and $x_{c_3} \approx 5.47 \times 10^{13}$, as shown in Figure 2a,b. It is similarly possible to study multiple crossovers for the case $M > 3$.

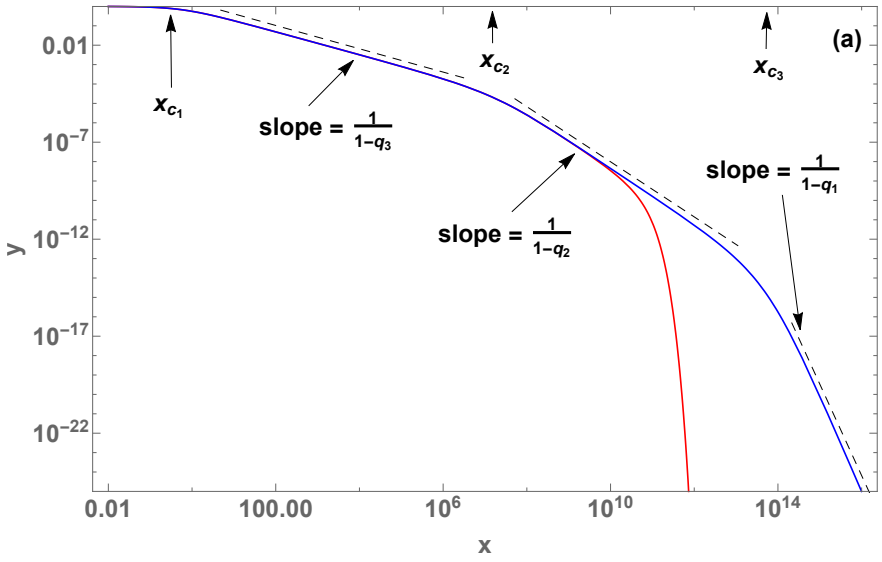

Figure 2. *Cont.*

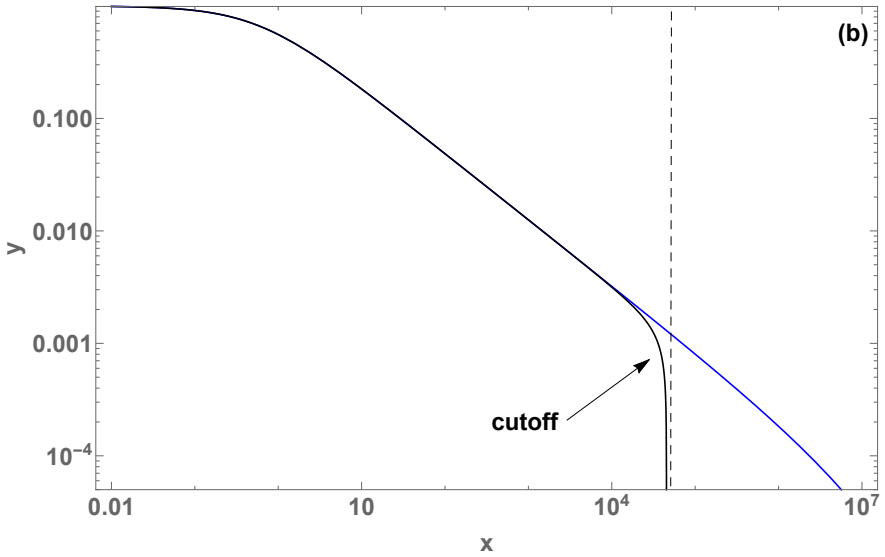

Figure 2. Crossovers in $y(x)$ for $M = 3$ (log-log plots) (**a**) between two curves with $(q_1, q_2) = (1, 1.7)$ (red curve), $(q_1, q_2) = (1.2, 1.7)$ (blue curve) respectively, both with $(q_3, a_1, a_2, a_3) = (2.7, 5 \times 10^{-11}, 1 \times 10^{-4}, 1)$, and (**b**) a change was done on the blue curve, with $q_1 = -1$ (black curve); the cutoff occurs at $x_{cutoff} \approx 4.48 \times 10^4$.

3. Linear Combination of Normalized q-Exponentials

For a linear combination of normalized q-exponentials, we consider a probability distribution function $P = P(x)$, $x \in X \subset \mathbb{R}^+$ such that:

$$P(x) = \sum_{k=1}^{M} b_k \, p_k(x) = \sum_{k=1}^{M} b_k \, \frac{e_{q_k}^{-\beta_{q_k} x}}{Z_{q_k}} \quad (q_1 \leq q_2 \leq \cdots \leq q_M < 2;\, \beta_{q_k} > 0\,, \forall\, k)\,, \tag{18}$$

with $\sum_{k=1}^{M} b_k = 1 \;\; (b_k \geq 0)$, $\{Z_{q_k}\}$ being normalization factors (the upper limit $q < 2$ emerges in order to $\{Z_{q_k}\}$ being finite). Those quantities are determined by imposing, for all $k \in \{1, ..., M\}$,

$$\int_0^{\infty} dx \, p_k(x) \;\; = \;\; 1 \;\; if \;\; q_k \geq 1\,, \tag{19}$$

$$\int_0^{\frac{1}{\beta_{q_k}(1-q_k)}} dx \, p_k(x) \;\; = \;\; 1 \;\; if \;\; q_k < 1\,. \tag{20}$$

It follows

$$Z_{q_k} = \frac{1}{\beta_{q_k}(2 - q_k)}\,, \;\; \forall\, q_k < 2\,. \tag{21}$$

Let us focus on two specific particular cases, namely $M = 2$ with $q_1 = q_2 \equiv q$, and $M = 3$ with $q_1 = q_2 = q_3 \equiv q$; $\beta_{q_1} \equiv \beta_1$, $\beta_{q_2} \equiv \beta_2$, $\beta_{q_3} \equiv \beta_3$, and $Z_{q_k} \equiv Z_k$. It follows that

$$p(x) = b_1 \frac{e_q^{-\beta_1 x}}{Z_1} + b_2 \frac{e_q^{-\beta_2 x}}{Z_2} \tag{22}$$

with $b_2 = 1 - b_1$, $1/Z_1 = \beta_1(2 - q)$, and $1/Z_2 = \beta_2(2 - q)$, and

$$p(x) = b_1 \frac{e_q^{-\beta_1 x}}{Z_1} + b_2 \frac{e_q^{-\beta_2 x}}{Z_2} + b_3 \frac{e_q^{-\beta_3 x}}{Z_3} \tag{23}$$

with $b_3 = 1 - b_1 - b_2$, $1/Z_1 = \beta_1(2 - q)$, $1/Z_2 = \beta_2(2 - q)$ and $1/Z_3 = \beta_3(2 - q)$. See Figures 3 and 4.

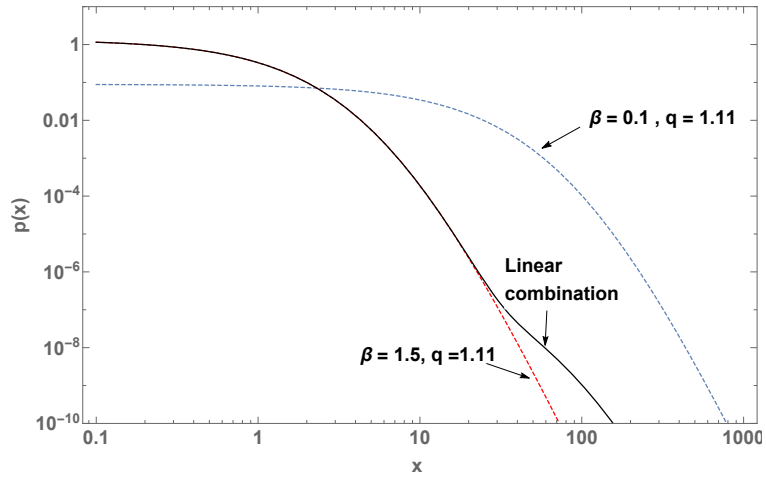

Figure 3. $p(x)$ (log-log plot) of three curves (case $M = 2$) with parameters $q = 1.11$ and $\beta = 0.1$ (blue dashed curve), $\beta = 1.5$ (red dashed curve), and their linear combination (black curve) with $b_1 = 1 \times 10^{-5}$ and $b_2 = 1 - b_1$.

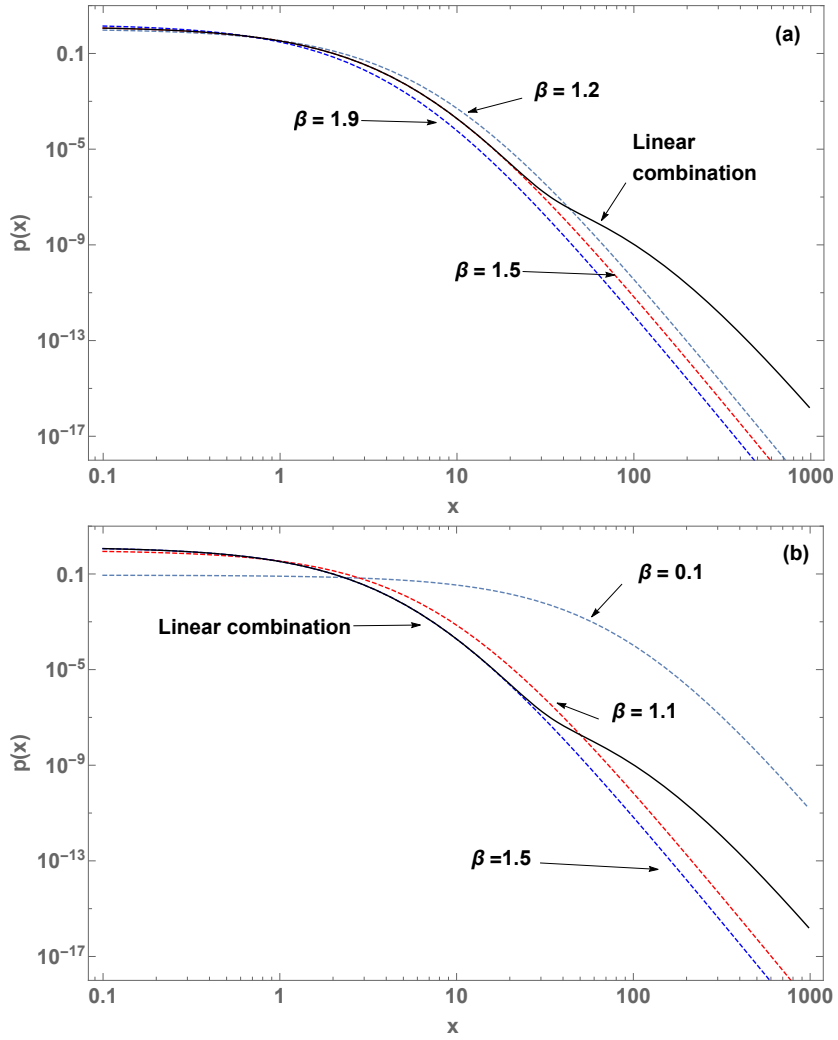

Figure 4. $p(x)$ (log-log plots) of four curves with parameters $q = 1.11$, $\beta = 1.9$ (blue dashed curve), $\beta = 1.5$ (red dashed curve), $\beta = 1.2$ (gray dashed curve), and their linear combination (black curve). (**a**) Four curves with $\beta = 1.5$ (blue dashed curve), $\beta = 1.1$ (red dashed curve), $\beta = 0.1$ (gray dashed curve) and their linear combination (black curve). (**b**) With $b_1 = 1 \times 10^{-5}$, $b_2 = 1 \times 10^{-3}$ and $b_3 = 1 - b_1 - b_2$, both with $q = 1.11$ (case $M = 3$).

In Figure 4 ($M = 3$), we fix the value $q_k = 1.11$ for $k = 1, 2, 3$. Another illustration of the linear combination consists of fixing the value $\beta_{q_k} = \beta$ for $k = 1, 2, 3$ and using three different values for q_k. In the case illustrated in Figure 5, the linear combination remains close to the curve corresponding to $(q, \beta) = (1.2, 0.1)$.

$$p(x) = b_1 \frac{e_{q_1}^{-\beta x}}{Z_{q_1}} + b_2 \frac{e_{q_2}^{-\beta x}}{Z_{q_2}} + b_3 \frac{e_{q_3}^{-\beta x}}{Z_{q_3}} \tag{24}$$

with $b_3 = 1 - b_1 - b_2$, $1/Z_{q_1} = \beta(2 - q_1)$, $1/Z_{q_2} = \beta(2 - q_2)$ and $1/Z_{q_3} = \beta(2 - q_3)$.

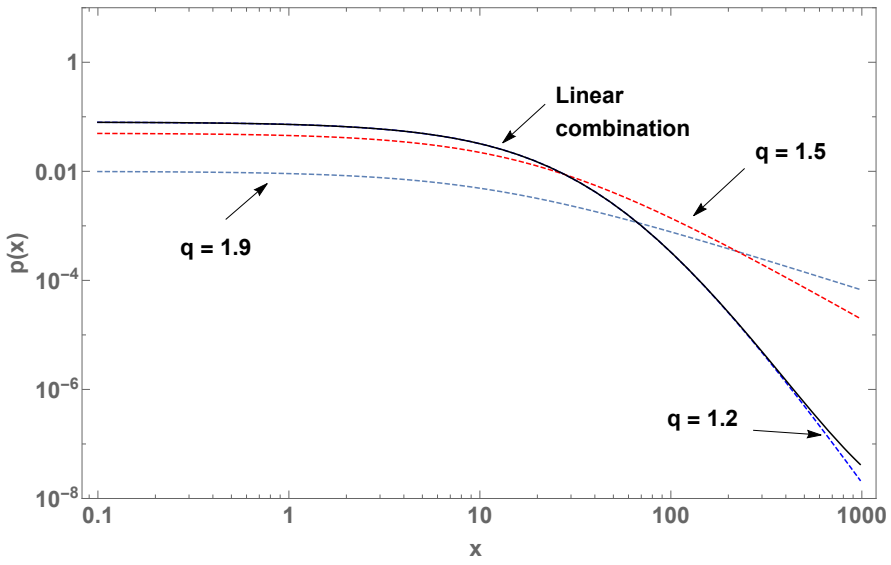

Figure 5. $p(x)$ (log-log plot) of four curves (case $M = 3$) with parameters $\beta = 0.1$, $q = 1.2$ (blue dashed curve), $q = 1.5$ (red dashed curve), $q = 1.9$ (gray dashed curve), and their linear combination (black curve) with $b_1 = 1 \times 10^{-5}$, $b_2 = 1 \times 10^{-3}$ and $b_3 = 1 - b_1 - b_2$.

Linear combinations of this kind (either of q-exponentials, or of q-Gaussians) have been fruitfully used in [4,13,24,25].

4. Linear Combination of q-Entropies

A linear combination of q-entropies can be written as follows:

$$S(\{p_i\}) = \sum_{k=1}^{M} c_k \, S_{q_k}(\{p_i\}) \quad (q_1 < q_2 < \cdots < q_M) \quad (c_k \geq 0) \, . \tag{25}$$

This expression is generically not normalized. If we happen to prefer normalization for some specific reason, it is enough to divide Equation (25) by $\sum_{k=1}^{M} c_k$.

With the constraints $\sum_i p_i - 1 = 0$ and $\sum_i p_i E_i - U = 0$, where U is the internal energy of the system and $\{E_i\}$ are the energy eigenvalues, we define the functional $f(\alpha_1, \alpha_2, \{p_i\})$ as follows:

$$f(\alpha_1, \alpha_2, \{p_i\}) \equiv \sum_{k=1}^{M} c_k \, S_{q_k}(\{p_i\}) + \alpha_1 \left(1 - \sum_i p_i\right) + \alpha_2 \left(U - \sum_i p_i E_i\right) . \tag{26}$$

Then, through extremization, we obtain

$$\frac{\partial}{\partial p_j} f = 0 = \sum_k c_k \left\{ \ln_{q_k} \frac{1}{p_j} - \left(\frac{1}{p_j}\right)^{1-q_k} \right\} - \alpha_1 - \alpha_2 E_j \tag{27}$$

hence

$$E(p_j) = -\frac{\alpha_1}{\alpha_2} + \frac{1}{\alpha_2}\sum_k c_k \left\{ \ln_{q_k} \frac{1}{p_j} - \left(\frac{1}{p_j}\right)^{1-q_k} \right\}. \tag{28}$$

We introduce convenient new variables, namely

$$\alpha_1 \equiv -\alpha_2 \mu, \ \alpha_2 \equiv \beta\,. \tag{29}$$

This enables us to express $X_j \equiv \beta(E_j - \mu)$ as an explicit function of p_j, namely

$$X_j = \sum_k c_k \left\{ \ln_{q_k} \frac{1}{p_j} - \left(\frac{1}{p_j}\right)^{1-q_k} \right\}. \tag{30}$$

The cutoff condition, whenever present, is given by $\lim_{p_j \to 0} X(p_j, q_1, q_2, \ldots, q_M) \equiv X_c(q_1, q_2, \ldots, q_M)$. For instance, for $M = 3$, we have (see Figure 6)

$$X_c(q_1, q_2, q_3) = \frac{c_1}{q_1 - 1} + \frac{c_2}{q_2 - 1} + \frac{c_3}{q_3 - 1}, \ (1 < q_1 \leq q_2 \leq q_3). \tag{31}$$

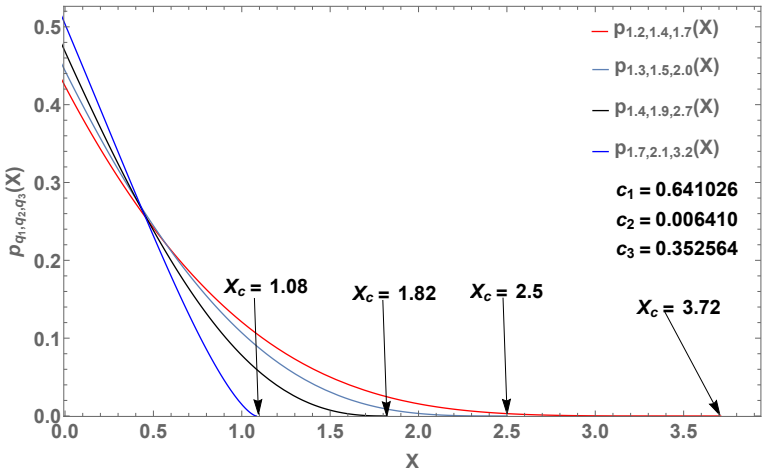

Figure 6. Four probability distributions $p_{q_1,q_2,q_3}(X)$ ($M = 3$) based on Equation (30) with $(c_1, c_2, c_3) = (0.641026, 0.006410, 0.352564)$. From (31), we respectively obtain the cutoff values $X_c = 1.08$ for $(q_1, q_2, q_3) = (1.7, 2.1, 3.2)$ (blue curve), 1.82 for $(q_1, q_2, q_3) = (1.4, 1.9, 2.7)$ (black curve), 2.50 for $(q_1, q_2, q_3) = (1.3, 1.5, 2.0)$ (gray curve) and $X_c = 3.72$ for $(q_1, q_2, q_3) = (1.2, 1.4, 1.7)$.

The $M = 2$ particular case of (25) has been focused on in [24]:

$$S(\{p_i\}) = c_1 S_{BG}(\{p_i\}) + c_2 S_q(\{p_i\}) \tag{32}$$

where one of the entropies is the BG entropy (i.e., $q_1 = 1$), and the other one $S_q(\{p_i\})$ corresponds to $q_2 \equiv q \neq 1$. Then, we have (see Figure 7)

$$p_j = \left\{ aW\left(A_q e^{-(q-1)X_j}\right) \right\}^{\frac{1}{q-1}} \tag{33}$$

where $W(z)$ is the Lambert function, implicitly defined by $We^W = z$ (see, for instance, [26]), $A_q \equiv \frac{1}{a} e^{-(q-1)\left(1 - \frac{c_2}{c_1(q-1)}\right)}$, $\alpha_1 \equiv -\mu\alpha_2$, $\beta \equiv \frac{\alpha_2}{c_1}$ and $X_j \equiv \beta(E_j - \mu)$ (this definition of β differs from that in Equation (29)), with $a \equiv \frac{c_1}{c_2 q} = \frac{c_1}{(1-c_1)q}$. A_q is determined via the normalization of the probabilities $\{p_j\}$, i.e.,

$$\sum_j p_j = \sum_j \left\{ aW\left(A_q e^{-(q-1)X_j}\right)\right\}^{\frac{1}{q-1}} = 1. \tag{34}$$

In other words, A_q implicitly depends on (q, c_1). Whenever appropriate, we may go to the continuum limit. If it is allowed to consider $X \geq 0$, we have

$$\int_0^\infty \left\{ aW\left(A_q e^{-(q-1)X}\right)\right\}^{\frac{1}{q-1}} dX = 1, \tag{35}$$

hence

$$qa^{-\frac{1}{q-1}} = W(A_q)^{\frac{1}{q-1}} \left[q + W(A_q)\right]. \tag{36}$$

This expression determines a as an explicit function of (q, A_q).

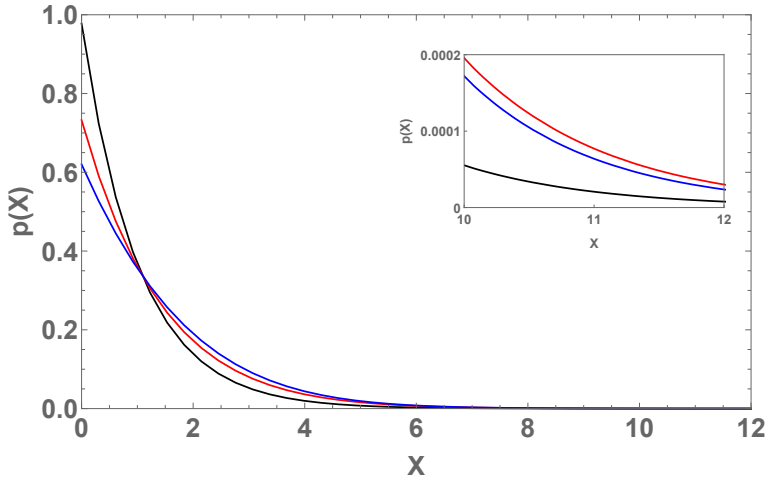

Figure 7. Three probability distributions $p(X)$ based on Equation (33) with $c_1 = 0.3$ and $q = 1.01$ hence $A_q = 0.0238786$ (black curve), $q = 1.2$ hence $A_q = 0.6798077$ (red curve), and $q = 1.5$ hence $A_q = 2.3025270$ (blue curve).

It is known that, in nonextensive statistical mechanics [27], the constraints under which the entropy is optimized might be chosen with escort distributions, namely, $\sum_i p_i - 1 = 0$ and $\frac{\sum_i p_i^q E_i}{\sum_i p_i^q} - U_q = 0$. We then have

$$\tilde{f}(\alpha_1, \alpha_2, \{p_i\}) \equiv c_1 S_{BG}(\{p_i\}) + c_2 S_q(\{p_i\}) + \alpha_1 \left(1 - \sum_i p_i\right) + \alpha_2 \left[U_q - \frac{\sum_i p_i^q E_i}{\sum_i p_i^q}\right] \tag{37}$$

hence

$$p_j = \left\{ a e_q^{(q-1)} W\left(B_q\, e_q^{-(q-1)X_j}\right)\right\}^{\frac{1}{q-1}}, \tag{38}$$

where $X_j \equiv \beta'(E_j - \mu)$ with β' defined as

$$\beta' \equiv \frac{\beta}{\sum_j p_j^q + (1-q)\beta U_q} \tag{39}$$

with $\beta \equiv \frac{\alpha_2}{c_1}$. Clearly, B_q is determined by

$$\sum_j p_j = \sum_k \left\{ a\, e_q^{(q-1)} W\left(B_q e_q^{-(q-1)X_j}\right)\right\}^{\frac{1}{q-1}} = 1\,. \tag{40}$$

Let us remind at this point that extremizing S_q with standard constraints is equivalent to extremizing S_{2-q} with escort constraints. The equivalence implies in doing the transformation $q \to 2-q$ [27,28].

Let us address now the concavity/convexity of $S\{p_i\}$. We illustrate with the linear combination of two ($M=2$) q-entropies with q_1 and q_2, assuming $p_1 \equiv p_2 \equiv \cdots \equiv p_{(W-1)} \equiv p$ and $p_W = 1-(W-1)p$. In other words, we consider

$$S_{q_1,q_2}(p) = c_1 \left[(W-1)p \ln_{q_1}\left(\frac{1}{p}\right) + (1-(W-1)p)\ln_{q_1}\left(\frac{1}{1-(W-1)p}\right)\right] + c_2 \left[(W-1)p \ln_{q_2}\left(\frac{1}{p}\right) + (1-(W-1)p)\ln_{q_2}\left(\frac{1}{1-(W-1)p}\right)\right]. \tag{41}$$

The study of concavity of (41) can be done in the (q_1, q_2) space, taking also into consideration the regions of non admissibility in which the entropy is neither concave nor convex.

We clearly note that when $W=3$ (see Figure 8b), the black region is reduced compared to the $W=2$ case (Figure 8a). This result tends to suggest that the black region tends to disappear at $W \to \infty$, while the pink (convex) region predominates.

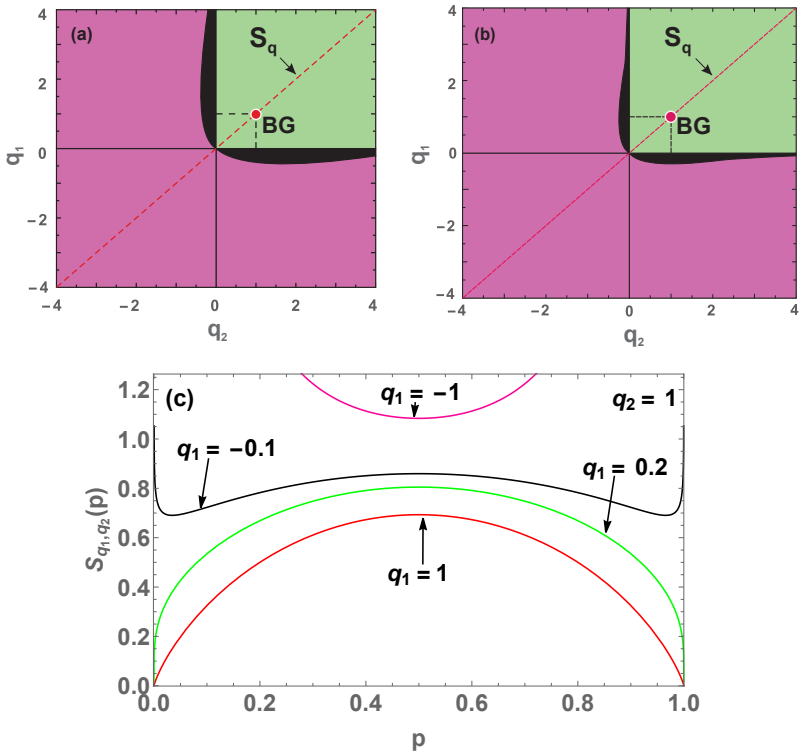

Figure 8. Concavity/convexity mapping for (41) with $(c_1, c_2) = (0.48, 0.52)$, $W=2$ (**a**) and $W=3$ (**b**). The green (pink) region represents all points whose entropy (41) is concave (convex). The black region represents all points whose entropy is neither concave nor convex, having two local minima points and a local maximum in between (a global maximum point at $p=0.5$ and divergences at $p=0$ and $p=1$). On the red point is localized the Boltzmann–Gibbs entropy and over the red dashed line cutting the origin, we have all the S_q entropies. On the concave (convex) region we have S_q, $q>0$ ($q<0$). (**c**) Four ($W=2$) entropies with $q_2=1$, and $q_1=1$ (blue curve), $q_1=0.2$ (green curve), $q_1=-0.1$ (black curve) and $q_1=-1$ (pink curve).

5. Other Departures—Two-Indices Entropies

We focus here on other type of departures from pure q-exponentials, originated now from two-indices nonadditive entropies which recover S_q as particular instances.

5.1. $S_{q,\delta}$

From [14], we have

$$S_{q,\delta} \equiv \sum_{i=1}^{W} p_i \left[\ln_q \frac{1}{p_i}\right]^{\delta} \quad (q \in \mathbb{R}; \delta > 0)\,. \tag{42}$$

We verify that $S_{q,1} = S_q$. Extremization of $S_{q,\delta}$ under usual constraints yields

$$E(p_j) = -\frac{\alpha_1}{\alpha_2} + \frac{1}{\alpha_2}\left\{\left[\ln_q \frac{1}{p_j}\right]^{\delta} - \delta\left(\frac{1}{p_j}\right)^{1-q}\left[\ln_q \frac{1}{p_j}\right]^{\delta-1}\right\}. \tag{43}$$

Through (29), we have

$$X_j = \left\{\left[\ln_q \frac{1}{p_j}\right]^{\delta} - \delta\left(\frac{1}{p_j}\right)^{1-q}\left[\ln_q \frac{1}{p_j}\right]^{\delta-1}\right\}. \tag{44}$$

Taking into account the transformation $q \to 2-q$ mentioned below Equation (40), the cutoff occurs for $q > 1$, and $X_c(q,\delta)$ is given by (see Figure 9)

$$X_c(q,\delta) = (q-1)^{-\delta} \quad (q > 1). \tag{45}$$

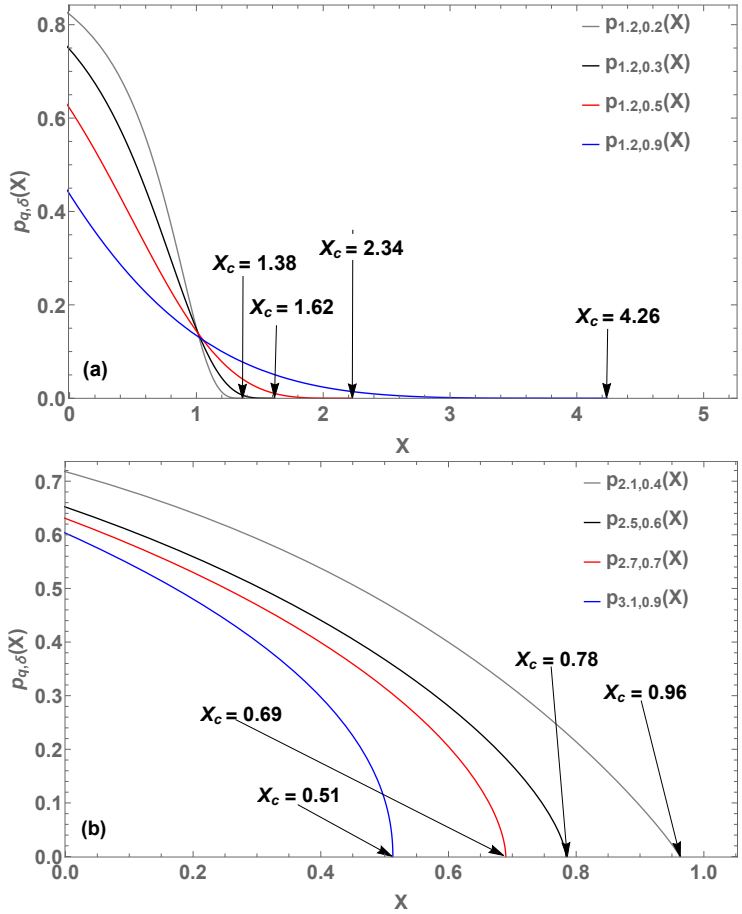

Figure 9. Illustrative probability distributions $p_{q,\delta}(X)$. (**a**) $q = 1.2$ and $\delta = 0.2$ hence, through (45), $X_c = 1.38$ (gray curve); $\delta = 0.3$, hence $X_c = 1.62$ (black curve); $\delta = 0.5$ hence $X_c = 2.34$ (red curve) and finally, $\delta = 0.9$ hence $X_c = 4.26$ (blue curve); (**b**) $(q,\delta) = (3.1, 0.9)$ hence $X_c = 0.51$ (blue curve); $(q,\delta) = (2.7, 0.7)$ hence $X_c = 0.69$ (red curve); $(q,\delta) = (2.5, 0.6)$ hence $X_c = 0.78$ (black curve); and $(q,\delta) = (2.1, 0.4)$ hence $X_c = 0.96$ (gray curve).

We verify that $p_{q,\delta}(X)$ is single-valued for $q \geq \delta$ and multi-valued otherwise.
Let us now consider the case $p_1 \equiv p_2 \equiv \cdots \equiv p_{(W-1)} \equiv p$ and $p_W = 1-(W-1)p$ hence

$$S_{q,\delta}(p) = (W-1)p\left[\ln_q\left(\frac{1}{p}\right)\right]^{\delta} + (1-(W-1)p)\left[\ln_q\left(\frac{1}{1-(W-1)p}\right)\right]^{\delta}, \tag{46}$$

where $p \in \left[0, \frac{1}{W-1}\right]$. This expression will help us to study the concavity/convexity of the entropy for increasing values of W. See Figures 10 and 11.

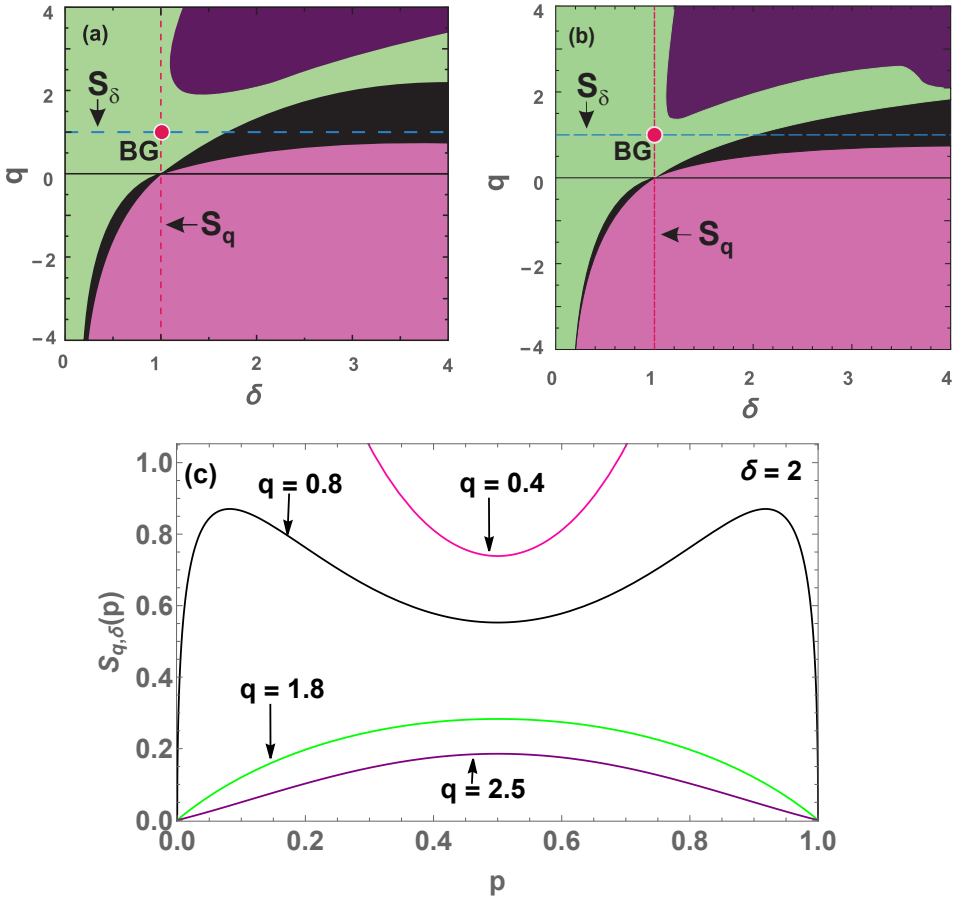

Figure 10. Concavity/convexity regions for $S_{q,\delta}$ (46) (**a**) $W = 2$. (**b**) $W = 3$. The green (pink) region represents all points whose entropy (41) is concave (convex). The black region represents all points whose entropy is neither concave nor convex, having two local maxima (inflexion) points and another local minimum (maximum) in between. The points of transition at $\delta = 2$ are: $q_c = 1/2$ (both $W = 2$ and $W = 3$) (pink $\leftrightarrow$ black); $q_c = 4/3$ ($W = 2$) and $q_c \sim 0.98$ ($W = 3$) (black $\leftrightarrow$ green) and $q_c = 2$ (both cases) (black $\leftrightarrow$ purple). At $q = 1$, we have the transition from non concave to concave at $\delta_c = 1 + \ln 2$ ($W = 2$) and for $W = 3$, we have $\delta_c < 1 + \ln 3$. The blue dashed horizontal line represents S_δ, while the red dashed vertical line represents all S_q entropies, and the red point is the BG entropy. (**c**) Four cases ($W = 2$) for $\delta = 2$ with the respective colors: $q = 0.4$ and $q = 1.8$ (convex and concave regions respectively); $q = 0.8$ (black region) and $q = 2.5$ (purple region) (non concave and non convex regions).

The black region is clearly reduced for $W = 3$ (see Figure 10b), but the purple region at, for example, $\delta = 3.8$ and $q = 2.15$, invades the concave region. It is not excluded that the purple region gradually expands with W in such way that it approaches the black region.

We noticed that an inadvertence occurred in [14]. Indeed, it was therein indicated that, for all entropies S_δ, it would be $\delta_c(W) = 1 + \ln W$, but this is not exactly so in some cases. As we verify

in what follows, we always have $\delta_c \in (\ln W, 1 + \ln W]$. Therefore, the formula in [14] constitutes an upper bound of δ_c.

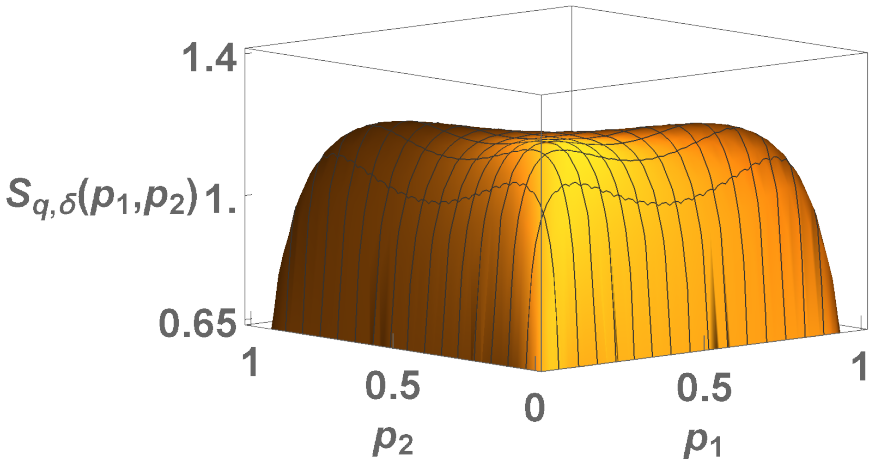

Figure 11. Plot for $S_{q,\delta}$ with $W = 3$, $q = 1$ and $\delta = 1 + \ln 3$. We clearly observe that $\delta_c = 1 + \ln W$ is not valid here, because in this value, the entropy is not concave, much less the values close to this.

The probability is limited by $p \geq \frac{1}{W-1}$. Numerically, we analyze the plot $1/\ln W \times \delta_c - \ln W$. If it was $\delta_c = 1 + \ln W$ for all entropies S_δ, we should obtain $\delta_c - \ln W = 1$ for all values of W, which is not the case.

The interpretation of δ_c is given by the transition green $\leftrightarrow$ black; no transition black $\leftrightarrow$ pink appears to exist.

We notice in Figures 10–13 that the divergence of δ_c in the limit $W \to \infty$ means that S_δ is concave in the thermodynamic limit for any positive δ.

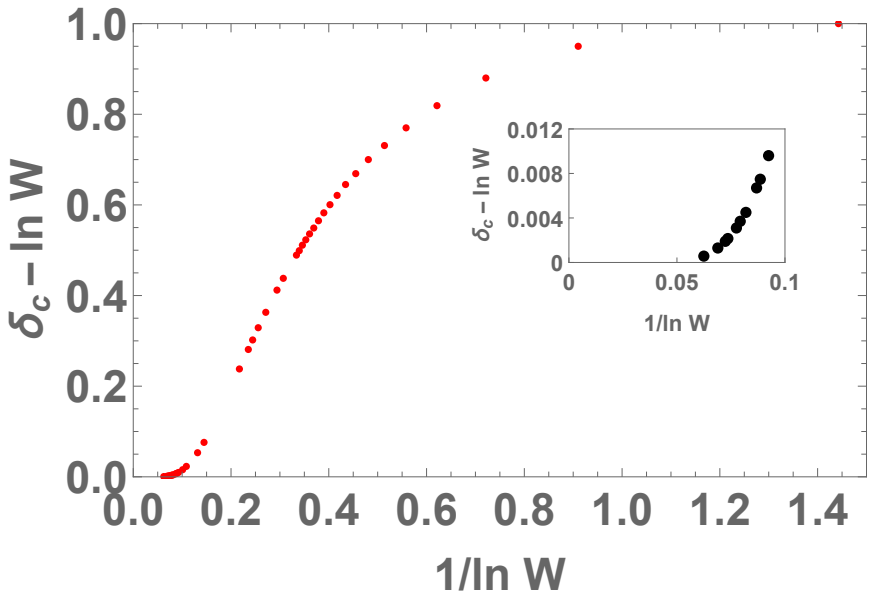

Figure 12. Plot for $1/\ln W \times \delta_c - \ln W$ with $W_{max} = 9 \times 10^6$. Here, $\delta_c \in (\ln W, 1 + \ln W]$. In the inset, we indicate the behavior of that function closer to origin.

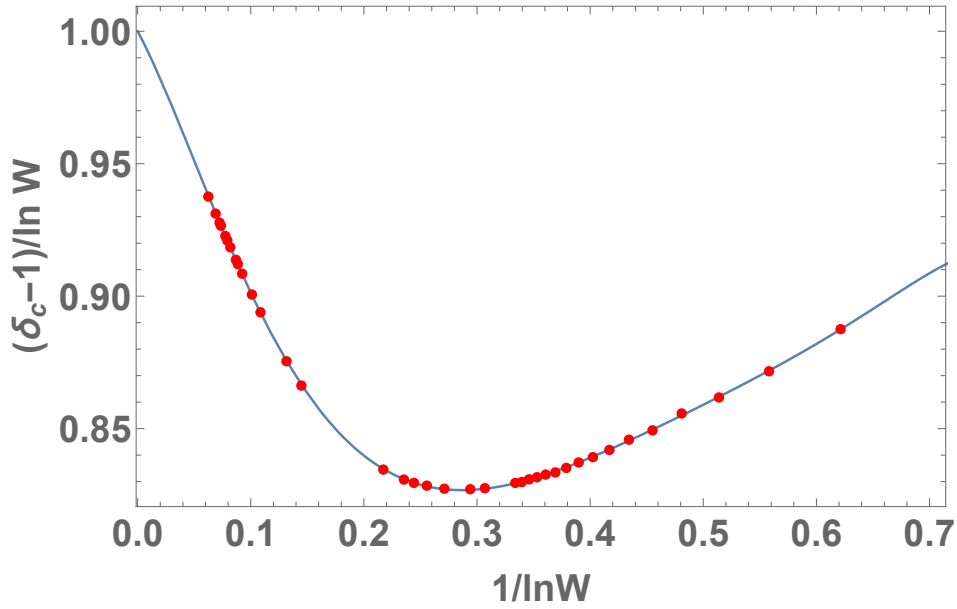

Figure 13. Plot for $1/\ln W \times (\delta_c - 1)/\ln W$ with $W_{max} = 9 \times 10^6$. The regression by excluding the $W = 2$ and $W = 3$ points yields an 8th degree polynomial of $x \equiv 1/\ln W$, namely $f(x) \approx 1 - 0.794252x - 6.20252x^2 + 60.9556x^3 - 223.39x^4 + 466.1x^5 - 588.297x^6 + 420.626x^7 - 130.677x^8$. It means that, when $W \to \infty$ we have $x \to 0$, thus $\lim_{x\to 0} f(x) = 1$, therefore $\delta_c \sim 1 + \ln W$ which diverges at infinity.

5.2. Borges–Roditi Entropy $S^{BR}_{q,q'}$

Borges and Roditi [15] extended the entropy S_q as follows:

$$S^{BR}_{q,q'} = \frac{\sum_{i=1}^{W} p_i^q - \sum_{i=1}^{W} p_i^{q'}}{q' - q}, \quad ((q, q') \in \mathbb{R}^2), \tag{47}$$

with $S^{BR}_{q,1} = S^{BR}_{1,q} = S_q$, where BR stands for Borges–Roditi; notice that $S^{BR}_{q,q'} = S^{BR}_{q',q}$.

Extremization with usual constraints, and using (29), we have:

$$X_j = \frac{1}{q' - q}\left(q p_j^{q-1} - q' p_j^{q'-1}\right). \tag{48}$$

For $q, q' < 1$, p monotonically decreases to zero when X increases to infinity. For $q, q' > 1$, p is multivalued, hence physically inadmissible. For $q < 1$, $q' > 1$ (hence, for $q > 1, q' < 1$), p is single-valued and exhibits a cutoff at X_c. See Figure 14 for typical examples.

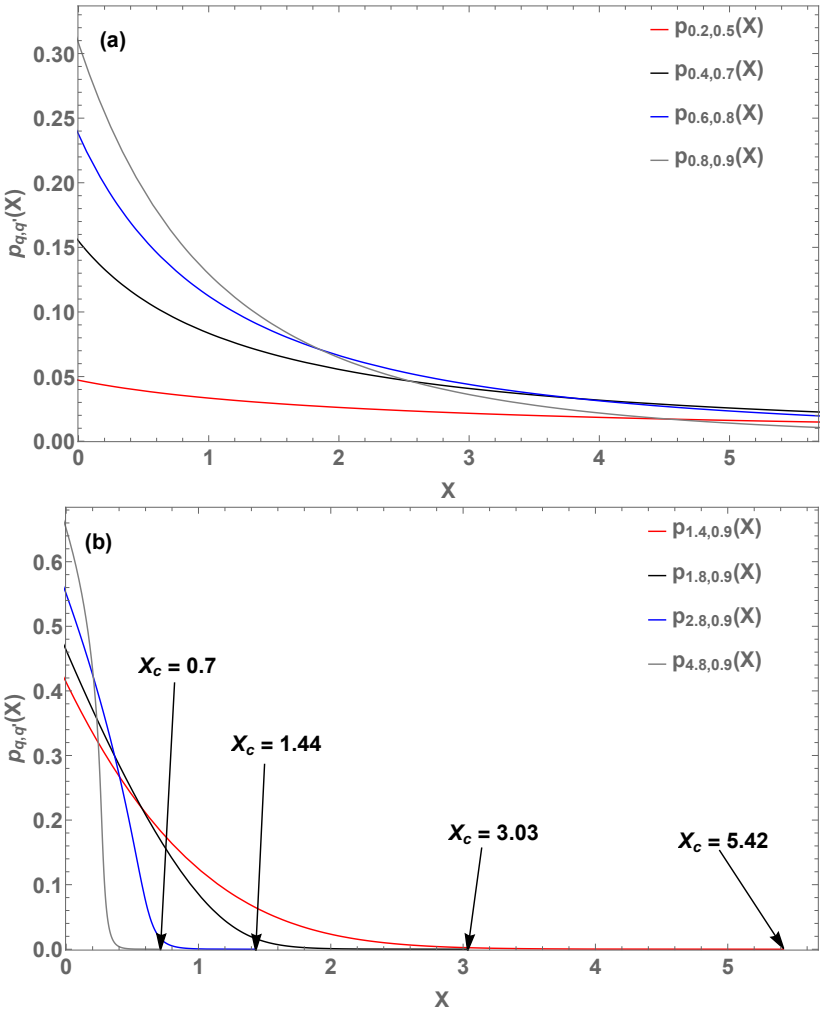

Figure 14. Eight illustrative Borges–Roditi probability distributions. (**a**) $(q, q') = (0.2, 0.5)$ (red curve); $(q, q') = (0.4, 0.7)$ (black curve); $(q, q') = (0.6, 0.8)$ (blue curve), and $(q, q') = (0.8, 0.9)$ (gray curve). (**b**) $(q, q', X_c) = (1.4, 0.9, 5.42)$ (red curve), $(q, q', X_c) = (1.8, 0.9, 3.03)$ (black curve), $(q, q', X_c) = (2.8, 0.9, 1.44)$ (blue curve), and $(q, q', X_c) = (4.8, 0.9, 0.7)$ (gray curve).

Let us focus now on the concavity of $S^{BR}_{q,q'}$. By considering the same case that led to Equation (46), we obtain here

$$S_{q,q'}(p) = \frac{1}{q' - q}\left[(W-1)p^q + (1-(W-1)p)^q - (W-1)p^{q'} - (1-(W-1)p)^{q'}\right]. \qquad (49)$$

The purple region undergoes a slight change whether we compare the Figure 15a ($W = 2$) and Figure 15b ($W = 3$), although it appears that the rectangular purple region at $W = 3$ does not increase for $W > 3$. Indeed, if it did that, it would affect the BG and S_q entropies whose convexity/concavity are known. With respect to the black region, the fact of that region shrinks from $W = 2$ to $W = 3$ suggests that it possibly disappears in $W \to \infty$.

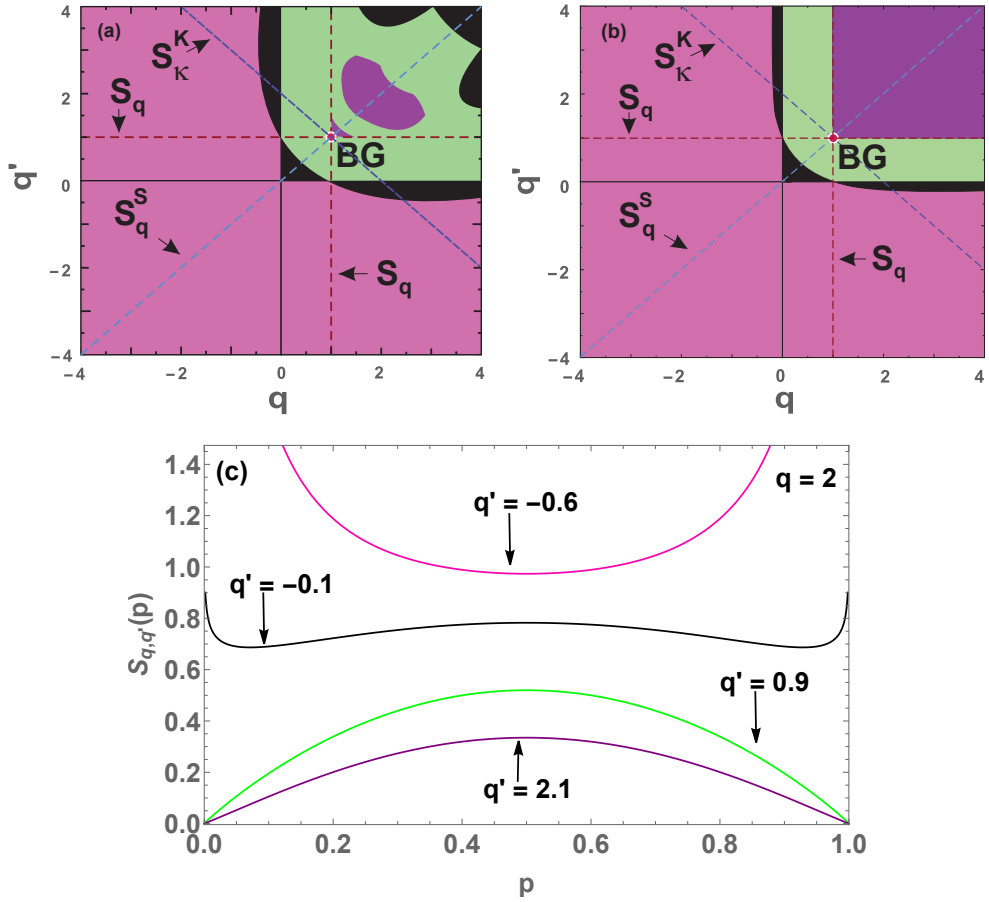

Figure 15. Concavity/convexity for $S^{BR}_{q,q'}$ (49) with (**a**) $W = 2$ and (**b**) $W = 3$. The green (pink) region represents all points whose entropy (49) is concave (convex). The black (purple) region represents all points whose entropy is neither concave nor convex, having two local maxima (inflexion) points and another local minimum (maximum) in between. The red dashed vertical lines represent all S_q entropies and the red point is the BG entropy, while the light (dark) blue lines represents all Shafee S^S_q (Kaniadakis S^K_κ) entropies [29,30]. (**c**) Four illustrative cases ($W = 2$) with $q = 2$ and its respective colors: $q' = -0.6$ and $q' = 0.9$ (pink and green regions respectively); $q = -0.1$ (black region) and $q = 2.1$ (purple region).

5.3. $S_{q,q'}$

On the basis of some algebraic properties, S_q has been generalized in [16,31,32]:

$$S_{q,q'} = \sum_{i=1}^{W} p_i \ln_{q,q'} \frac{1}{p_i} \tag{50}$$

with

$$\ln_{q,q'} z \equiv \frac{1}{1-q'}\left[\exp\left(\frac{1-q'}{1-q}(z^{1-q}-1)\right)-1\right]. \tag{51}$$

We verify that $\ln_{q,1} = \ln_{1,q} = \ln_q$, hence $S_{q,1} = S_{1,q} = S_q$. with $S_{q,1} = S_{1,q} = S_q$. Clearly, we can reformulate (51) in terms of $\ln_q$ such that

$$\ln_{q,q'} z = \frac{1}{1-q'}\left[\exp\left((1-q')\ln_q z\right)-1\right]. \tag{52}$$

The reformulated version of the extremized entropy $S_{q,q'}$ is written as

$$X_j = \exp\left((1-q')\ln_q \frac{1}{p_j}\right)\left[\frac{1}{1-q'} - \left(\frac{1}{p_j}\right)^{1-q}\right] - \frac{1}{1-q'} \tag{53}$$

The cutoff equation $X_c(q,q')$ is given by

$$X_c(q,q') = \frac{1}{1-q'}\left[e^{-\frac{1-q'}{1-q}} - 1\right], \; q > 1. \tag{54}$$

For $q > 1$ and $0 < q' < 1$, p is single-valued and exhibits a cutoff at X_c (see Figure 16). For $q, q' < 1$, p is multi-valued, hence, it is inadequate for physical purposes. For $0 < q < 1$ and $q' > 1$, p exhibits clearly a cutoff.

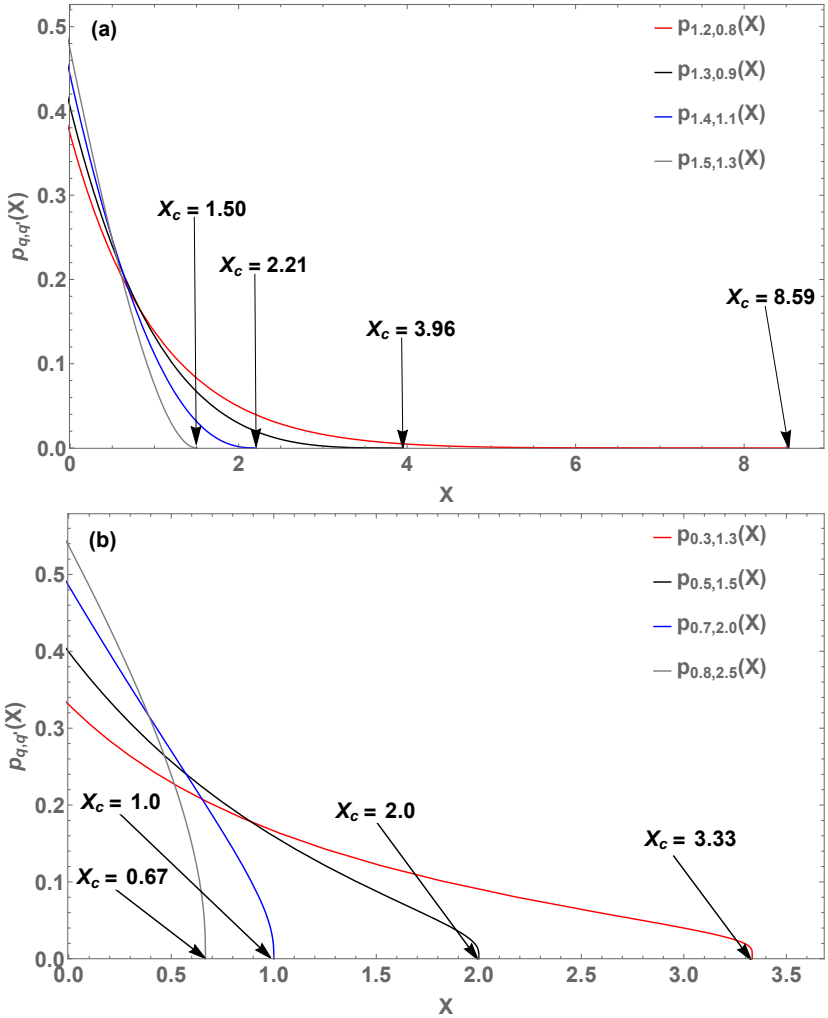

Figure 16. Eight illustrative probability distributions $p_{q,q'}(X)$. (**a**) $(q,q',X_c) = (1.5,1.3,1.5)$ (gray curve), $(q,q',X_c) = (1.4,1.1,2.21)$ (blue curve), $(q,q',X_c) = (1.3,0.9,3.96)$ (black curve), and $(q,q',X_c) = (1.2,0.8,8.59)$ (red curve). (**b**) $(q,q',X_c) = (0.8,2.5,0.67)$ (gray curve), $(q,q',X_c) = (0.7,2.0,1.0)$ (blue curve), $(q,q',X_c) = (0.5,1.5,2.06)$ (black curve), and $(q,q',X_c) = (0.3,1.3,3.33)$ (red curve).

Analogously to (46), we write the Equation (50) as

$$S_{q,q'}(p) = (W-1)p\ln_{q,q'}\left(\frac{1}{p}\right) + (1-(W-1)p)\ln_{q,q'}\left(\frac{1}{1-(W-1)p}\right). \tag{55}$$

In Figure 17a,b, we observe that the purple region appears to remain the same for all $W \geq 2$. In contrast, the black region for $W = 3$ is slightly smaller than that for $W = 2$, which suggests that, in $W \to \infty$, such a region might disappear. We checked for large values of W, and this scenario is confirmed. This happens in two different ways: the black region close to the BG point gradually disappears, being replaced by the pink (convex) region, and the black region in the negative part of q' also disappears, being replaced by the green (concave) region.

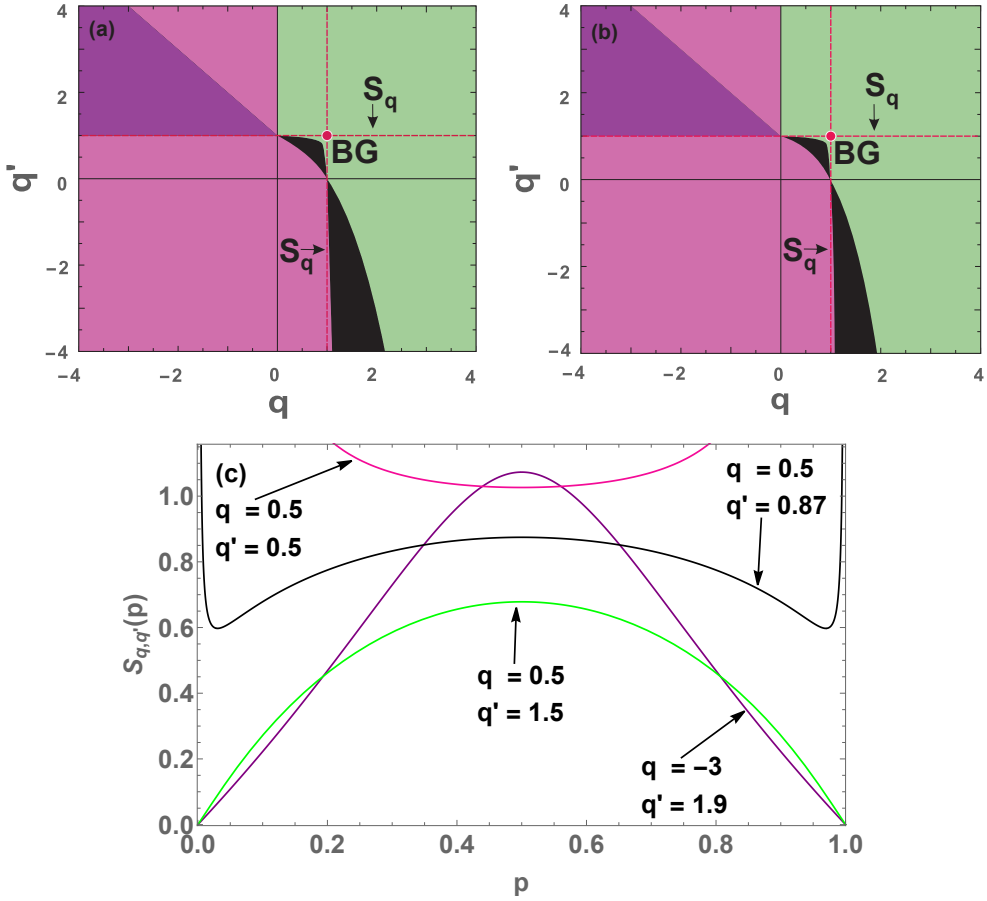

Figure 17. Concavity/convexity for $S_{q,q'}$ (55) with (**a**) $W = 2$ and (**b**) $W = 3$. The green (pink) region represents all points whose entropy (55) is concave (convex). The black (purple) region represents all points whose entropy is neither concave nor convex, having two local maxima (inflexion) points and another local minimum (maximum) in between. The red dashed vertical line represents all S_q entropies and the red point is the BG entropy. (**c**) Four cases ($W = 2$) with the respective colors: with $q = 0.5$, $q' = 0.5$ and $q' = 1.5$ (pink and green regions) and $q' = 0.87$ (black region), and $(q', q) = (1.9, -3)$ (purple region).

6. Conclusions

In summary, we have explored here various mathematical properties related to extensions of q-exponentials and q-entropies, including some double-index nonadditive entropies.

In the case of crossover statistics (Equation (7)), there are multiple changes in the slopes of the corresponding log-log plots. The values of the abscissa at which the relevant quantities make crossovers between two successive regimes are characterized by x_c, analytically calculated in all cases, as illustrated in Figures 1 and 2.

When we consider linear combinations of normalized q-exponentials, we may focus on the influence of the q_k's and of the β_k's in Equation (18). For a single value of β_k and various values for the q_k's, the result might be close to one of the q-exponentials, whereas if we adopt a single value of q_k

and various values for the β_k's, the outcome might be sensibly different from all the q-exponentials, as illustrated in Figures 3–5.

With respect to the linear combination of q-entropies, it is generically impossible to have the probability distribution p_j in Equation (30) as an explicit function of X_j. Notice, however, that we do have X_j as an explicit function of p_j. This is in contrast with the case where we have linear combinations of the normalized q-exponentials. The final results for these two types of linear combinations clearly differ, as first shown in [24]. Let us emphasize that, consistently, the operations of linearly combining and entropic extremization do not commute.

In addition to that, for the linear combination of two nonadditive entropies (case $M = 2$), as well as for the three double-index nonadditive entropies (namely, $S_{q,\delta}$, $S^{BR}_{q,q'}$ and $S_{q,q'}$), we have studied their convexity/concavity in the indices-space. The results depend naturally on the total number of states (W). The limit $W \to \infty$ is particularly interesting, since it corresponds to the thermodynamical limit. We verify that, in the case of a linear combination of two q-entropies ($M = 2$), the concave region remains one and the same for all values of W. Indeed, the value of W only affects the size of the convex region, as illustrated in Figure 8. It seems plausible that, in the $W \to \infty$ limit, the only possibilities which remain are either concave or convex. In what concerns $S_{q,\delta}$, $S^{BR}_{q,q'}$ and $S_{q,q'}$, regions in the indices-space exist, for a given value of W, where the entropy is concave, or convex, or none of them, as illustrated in Figures 10, 15 and 17. For all these three entropies, the region which is neither concave nor convex does not disappear even for $W \to \infty$. In particular, we have studied in detail the case of S_δ ($q = 1$ and $\delta > 0$), and have obtained that convexity never emerges, $\forall\delta$, $\forall W$. A critical value $\delta_c(W)$ exists such that S_δ is concave for $\delta < \delta_c(W)$ and neither concave nor convex for $\delta > \delta_c(W)$; moreover, in the $W \to \infty$ limit, we verify that $\delta_c(W) \sim \ln W$. The results displayed in the present paper could hopefully guide the use of entropies differing from S_q for large classes of natural, artificial and social complex systems.

Author Contributions: Conceptualization, C.T.; methodology, C.T.; software, H.S.L.; validation, H.S.L.; formal analysis, C.T.; investigation, H.S.L. and C.T.; resources, H.S.L. and C.T.; data curation, H.S.L. and C.T.; writing–original draft preparation, H.S.L. and C.T.; writing–review and editing, H.S.L. and C.T.; visualization, H.S.L. and C.T.; supervision, C.T.; project administration, C.T.; funding acquisition, H.S.L. and C.T. All authors have read and agreed to the published version of the manuscript.

Funding: This research was funded by CNPq-Conselho Nacional de Desenvolvimento Cientifico e Tecnologico and by FAPERJ—Fundacao Carlos Chagas Filho de Amparo a Pesquisa do Estado do Rio de Janeiro.

Acknowledgments: We acknowledge related exchanges with Nobar Baella, Rouhollah Ebrahimi, and Hamid-Reza Rastegar, at early stages of this work.

Conflicts of Interest: The authors declare no conflicts of interest. The funders had no role in the design of the study, in the collection, analysis, or interpretation of data, in the writing of the manuscript, or in the decision to publish the results.

References

1. Saxena, R.K.; Mathai, A.M.; Haubold, H.J. Astrophysical thermonuclear functions for Boltzmann—Gibbs statistics and Tsallis statistics. *Phys. A* **2004**, *344*, 649–656. [CrossRef]
2. Plastino, A.R.; Plastino, A. Stellar polytropes and Tsallis' entropy. *Phys. Lett. A* **1992**, *174*, 384–386. [CrossRef]
3. Ausloos, M.; Petroni, F. Tsallis non-extensive statistical mechanics of El Niño southern oscillation index. *Phys. A* **2007**, *373*, 721–736. [CrossRef]
4. Bogachev, M.I.; Kayumov, A.R.; Bunde, A. Universal internucleotide statistics in full genomes: A footprint of the DNA structure and packaging? *PLoS ONE* **2014**, *9*, e112534. [CrossRef]
5. Borland, L. Closed form option pricing formulas based on a non-Gaussian stock price model with statistical feedback. *Phys. Rev. Lett.* **2002**, *89*, 098701. [CrossRef]
6. Deppman, A.; Megias, E.; Menezes, D.P. Fractals, non-extensive statistics, and QCD. *Phys. Rev. D* **2020**, *101*, 034019. [CrossRef]
7. Combe, G.; Richefeu, V.; Stasiak, M.; Atman, A.P.F. Experimental validation of nonextensive scaling law in confined granular media. *Phys. Rev. Lett.* **2015**, *115*, 238301. [CrossRef]

8. Lutz, E.; Renzoni, F. Beyond Boltzmann-Gibbs statistical mechanics in optical lattices. *Nat. Phys.* **2013**, *9*, 615–619. [CrossRef]
9. Tsallis, C. Possible generalization of Boltzmann-Gibbs statistics. *J. Stat. Phys.* **1988**, 52, 479–487. [CrossRef]
10. Tsallis, C. *Introduction to Nonextensive Statistical Mechanics—Approaching a Complex World*; Springer: New York, NY, USA, 2009.
11. A Regularly Updated Bibliography. Available online: http://tsallis.cat.cbpf.br/biblio.htm (accessed on 14 September 2020).
12. Tsallis, C.; Bemski, G.; Mendes, R.S. Is re-association in folded proteins a case of nonextensivity? *Phys. Lett. A* **1999**, *257*, 93–98. [CrossRef]
13. Tirnakli, U.; Borges, E.P. The standard map: From Boltzmann-Gibbs statistics to Tsallis statistics. *Sci. Rep.* **2016**, *6*, 23644. [CrossRef] [PubMed]
14. Tsallis, C.; Cirto, L.J.L. Black hole thermodynamical entropy. *Eur. Phys. J. C* **2013**, *73*, 2487. [CrossRef]
15. Borges, E.P.; Roditi, I. A family of non-extensive entropies. *Phys. Lett. A* **1998**, *246*, 399. [CrossRef]
16. Schwammle, V.; Tsallis, C. Two-parameter generalization of the logarithm and exponential functions and Boltzmann-Gibbs-Shannon entropy. *J. Math. Phys.* **2007**, *48*, 113301. [CrossRef]
17. Tsekouras, G.A.; Tsallis, C. Generalized entropy arising from a distribution of q-indices. *Phys. Rev. E* **2005**, *71*, 046144. [CrossRef] [PubMed]
18. Oikonomou, T.; Provata, A. Non-extensive trends in the size distribution of coding and non-coding DNA sequences in the human genome. *Eur. Phys. J. B* **2006**, *50*, 259–264. [CrossRef]
19. Bakar, B.; Tirnakli, U. Analysis of self-organized criticality in Ehrenfest's dog-flea model. *Phys. Rev. E* **2009**, *79*, 040103(R). [CrossRef]
20. Celikoglu, A.; Tirnakli, U.; Queiros, S.M.D. Analysis of return distributions in the coherent noise model. *Phys. Rev. E* **2010**, *82*, 021124. [CrossRef]
21. Bakar, B.; Tirnakli, U. Return distributions in dog-flea model revisited. *Phys. A* **2010**, *389*, 3382–3386. [CrossRef]
22. Planck, M. Ueber irreversible Strahlungsvorgänge. *Ann. D Phys.* **1900**, *1*, 69–122. [CrossRef]
23. Planck, M. Zur Theorie des Gesetzes der Energieverteilung im Normalspectrum. *Verhandl. Dtsch. Phys. Ges.* **1900**, *2*, 237–245.
24. Sicuro, G.; Bagchi, D.; Tsallis, C. On the connection between linear combination of entropies and linear combination of extremizing distributions. *Phys. Lett. A* **2016**, *380*, 2025–2030. [CrossRef]
25. Ruiz, G.; Tirnakli, U.; Borges, E.P.; Tsallis, C. Statistical characterization of the standard map. *J. Stat. Mech.* **2017**, *2017*, 063403. [CrossRef]
26. da Silva, G.F.T.; Moreira, A.A.; Nobre, F.D.; Curado, E.M.F. Thermostatistics of overdamped motion of interacting particles. *Phys. Rev. Lett.* **2010**, *105*, 260601.
27. Tsallis, C.; Mendes, R.S.; Plastino, A.R. The role of constraints within generalized nonextensive statistics. *Phys. A* **1998**, *261*, 534–554. [CrossRef]
28. Ferri, G.L.; Martinez, S.; Plastino, A. Equivalence of the four versions of Tsallis' statistics. *J. Stat. Mech. Theory Exp.* **2005**, *2005*, P04009. [CrossRef]
29. Shafee, F. Lambert function and a new non-extensive form of entropy. *IMA J. Appl. Math.* **2007**, *72*, 785–800. [CrossRef]
30. Kaniadakis, G. Statistical mechanics in the context of special relativity. *Phys. Rev. E* **2002**, *66*, 056125. [CrossRef]
31. Asgarani, S.; Mirza, B. Probability distribution of (Schwammle and Tsallis) two-parameter entropies and the Lambert W-function. *Phys. A* **2008**, *387*, 6277–6283. [CrossRef]
32. Corcino, C.B.; Corcino, R.B. Logarithmic generalization of the Lambert W function and its applications to adiabatic thermostatics of the three-parameter entropy. *arXiv* **2020**, arXiv:2011.04283.